

11-25-2009

# Spatially resolved in situ FTIR analysis of CO adsorption and reaction on Pt/SiO<sub>2</sub> in a silicon microreactor

Chung K. Tan

*Purdue University - Main Campus, tancc@purdue.edu*

Nicholas W. Delgass

*Purdue University - Main Campus, delgass@purdue.edu*

Chelsey Baertsch

*Purdue University - Main Campus, baertsch@purdue.edu*

Follow this and additional works at: <http://docs.lib.purdue.edu/nanopub>



Part of the [Nanoscience and Nanotechnology Commons](#)

Tan, Chung K.; Delgass, Nicholas W.; and Baertsch, Chelsey, "Spatially resolved in situ FTIR analysis of CO adsorption and reaction on Pt/SiO<sub>2</sub> in a silicon microreactor" (2009). *Birck and NCN Publications*. Paper 569.

<http://docs.lib.purdue.edu/nanopub/569>

This document has been made available through Purdue e-Pubs, a service of the Purdue University Libraries. Please contact [epubs@purdue.edu](mailto:epubs@purdue.edu) for additional information.



## Spatially resolved *in situ* FTIR analysis of CO adsorption and reaction on Pt/SiO<sub>2</sub> in a silicon microreactor

Chung Kwang Christopher Tan<sup>a,b</sup>, W. Nicholas Delgass<sup>a</sup>, Chelsey D. Baertsch<sup>a,b,\*</sup>

<sup>a</sup> School of Chemical Engineering, Purdue University, West Lafayette, IN 47907-2100, USA

<sup>b</sup> Birck Nanotechnology Center, Purdue University, West Lafayette, IN 47907-2057, USA

### ARTICLE INFO

#### Article history:

Received 21 April 2009

Received in revised form 8 September 2009

Accepted 8 September 2009

Available online 15 September 2009

#### Keywords:

Focal plane array

MEMS

Microreactor

*In situ* spectroscopy

Spatial resolution

CO oxidation

### ABSTRACT

The design, fabrication and testing of a microreactor-FTIR imaging system is shown and used for the first time to demonstrate the ability to obtain *in situ* transmission FTIR analysis of working catalysts with both spatial and temporal resolution. MEMS (MicroElectroMechanical Systems) and microfabrication technologies were used to design and fabricate a microreactor with geometric and optical properties ideal for coupling with a high-throughput transmission FPA-FTIR system. CO adsorption and oxidation on Pt/SiO<sub>2</sub> were used as a model catalyst system. Propagation of adsorbed species down the length of the microreactor was observed and fractional coverages were quantified during pulsed chemisorption experiments. The amount of adsorbed CO was also differentiated at different positions in the microreactor as a function of time during oxidation of the stored surface species.

© 2009 Elsevier B.V. All rights reserved.

### 1. Introduction

Not all catalytic reaction processes are designed to run at steady state. Many require transient and/or cyclical operation and thus reactive surface species are transient in nature. Characterizing the mechanism of such catalytic reactions requires *in situ* transient methods. Additionally, many transient/cyclic catalytic processes are operated using a monolith tube reactor in practice, and thus characterization of their mechanism and performance requires spatially and temporally resolved analytical tools to monitor the catalyst surface and reactive species as a function of position on the catalyst surface and in the reactor channel. The NO<sub>x</sub> storage reduction (NSR) process developed by Toyota [1] for NO<sub>x</sub> removal [2–6] from lean burn diesel engines is an example of such a cyclic process requiring both temporal and spatial resolution for *in situ* catalyst surface analysis.

Spatially Resolved Mass Spectrometry (SpaciMS) [7,8], has been used to study the identity of gas phase species within a monolith reactor during NSR reactions using small capillary probes inserted into the monolith. Such measurements capture only finite points in the reactor and provide no information related to the catalyst

surface or reactive intermediates. No *in situ* analytical or spectroscopic method has previously been demonstrated capable of characterizing the presence and relative abundance of reactive surface intermediates within an operating tube reactor as a function of both time and position along a reaction channel.

High-throughput spectroscopic systems have been reported [9–15], but these are mostly used for analyzing multiple reactors in parallel, not for analyzing different catalyst surface positions during a transient reaction. Our experimental transmission FPA-FTIR system extends the use of the same technology developed by Snively and Lauterbach [9] and previously used for the high-throughput, parallel analysis of catalyst libraries and pellets. Here we demonstrate the use of a silicon fabricated microreactor, coupled with a custom infrared imaging system, to allow observation of the propagation and consumption of adsorbed CO on a Pt/SiO<sub>2</sub> catalyst surface down the length of the microreactor during CO adsorption and oxidation. CO oxidation has been widely studied on Pt supported on a variety of materials [16–18]. This well studied system is used as a basis for characterizing and demonstrating our microreactor-imaging system presented here.

Using silicon as a reactor substrate and microfabrication technologies to process that substrate provides a means for realizing a microreactor with required optical and geometric properties for transmission infrared spectroscopy of working transient catalyst surfaces in microchannels. Silicon and glass microfabricated reactors have previously been used to enable *in situ* Infrared, UV–visible, and Raman spectroscopic analysis of

\* Corresponding author at: School of Chemical Engineering, Purdue University, 480 Stadium Mall Drive, West Lafayette, IN 47907-2100, USA. Tel.: +1 765 496 7826; fax: +1 765 494 0805.

E-mail address: [baertsch@purdue.edu](mailto:baertsch@purdue.edu) (C.D. Baertsch).

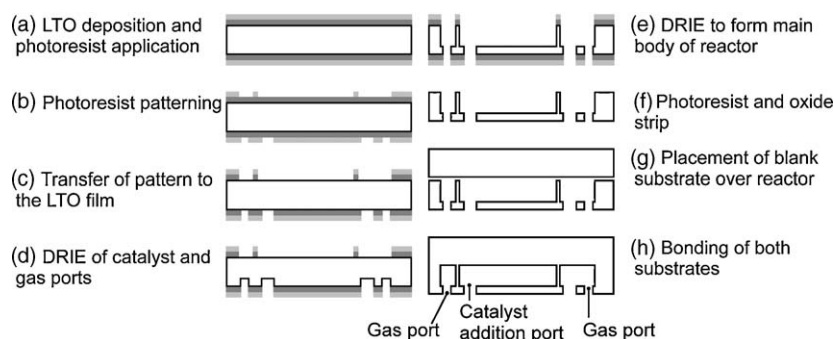


Fig. 1. Microreactor fabrication procedure.

liquids and solids [19–22]; however, without the spatial resolution provided by the FPA system used here.

Microsystem designs developed in a similar fashion as the one presented here would enable the study of catalysts operating in a geometry mimicking monolith channels for automotive and environmental treatment applications. For example, the formation, propagation and disappearance of surface species during NSR storage and reduction in parallel silicon microchannels channels could be observed. Such knowledge would allow researchers to better understand and verify the mechanistic models that have been developed and studied to describe the NSR process [23–29] and used to control diesel engine systems to enable a reduction in vehicular pollution.

## 2. Experimental

### 2.1. Microreactor fabrication

The dimension of the main reactor channel is a  $10\text{ mm} \times 10\text{ mm}$  square with a depth of  $400\text{ }\mu\text{m}$  to allow sufficient area for *in situ* spectroscopic characterization. The design includes two rows of catalyst retention posts, one near the inlet and one near the outlet, to keep powered catalyst within the reaction channel. Each row contains 334 posts ( $20\text{ }\mu\text{m}$  long by  $20\text{ }\mu\text{m}$  wide and spaced  $10\text{ }\mu\text{m}$ ). Two rectangular ports ( $1\text{ mm} \times 3\text{ mm}$ ) allow catalyst loading into the main channel and two square ports ( $1\text{ mm} \times 1\text{ mm}$ ) allow for gas inlet/outlet.

Fabrication began for the main reactor body with a double-sided polished  $500\text{ }\mu\text{m}$  thick,  $100\text{ mm}$  diameter undoped float-zone (FZ) grown silicon wafer (Silicon Valley Microelectronics), which provides  $>50\%$  transmission of  $25\text{--}250\text{ }\mu\text{m}$  radiation to enable *in situ* FTIR spectroscopic analysis in the microreactor. Standard microelectronics and MEMS processing methods were used for microreactor fabrication [30,31]. 4 reactors are processed on each Si wafer. A  $1.8\text{ }\mu\text{m}$  thick low temperature oxide (LTO) layer was grown at  $410\text{ }^\circ\text{C}$  to serve as a mask for the deep silicon etch (Fig. 1(a)). Photolithography was used to define the main reactor body as well as ports for catalyst loading and gas inlet/outlet (Fig. 1(b)) and the LTO was etched using a 6:1 buffered oxide etch (BOE) solution (Fig. 1(c)). The backside silicon of the reactor body was processed first using a Surface Technology Systems deep reactive ion etcher (STS-DRIE) to etch  $\sim 100\text{ }\mu\text{m}$  (Fig. 1(d)). The topside silicon was then etched  $\sim 400\text{ }\mu\text{m}$ , or until the backside ports were completely etched through to the main body of the reactor (Fig. 1(e)). Photoresist and LTO layers were removed using acetone and BOE, respectively (Fig. 1(f)). Prior to bonding, both the processed reactor wafer and a second double-side polished undoped FZ silicon wafer were cleaned using a piranha bath mixed at room temperature ( $2:1\text{ H}_2\text{SO}_4:\text{H}_2\text{O}_2$  by volume) followed by treatment in a 10 min oxygen plasma at 1.5 Torr and 150 W (Branson barrel etcher). The two substrates were then subjected to

a standard RCA-1 clean [32] for 15 min, rinsed and dried, and contacted by applying pressure to the center of the wafer pair (Fig. 1(g)). The contacted wafer system was annealed at  $\sim 1000\text{ }^\circ\text{C}$  for 90 min in an inert environment to strengthen the bond interface [33] (Fig. 1(h)).

A photograph of the fabricated microreactor is shown in Fig. 2, showing the microreactor channel and ports for gas feeds and catalyst loading. Throughout this paper, all characterizations were carried out at room temperature, although heating elements may be easily integrated into the device either with an external heater mounted within the package [34] or with on-chip resistive heating elements [35,36] to reach relevant temperatures for catalysis studies. Thermal changes in the system should have no adverse effect on the collection of FTIR spectra, even for reactions including NSR for which thermal spikes and transients are expected, as exemplified by spectra collected in transmission at elevated temperatures over pressed self-supporting catalyst disks by Fanson et al. [37].

### 2.2. COMSOL simulations

To capture the nature of gas flows in the silicon microreactor, COMSOL Multiphysics<sup>®</sup> 3.2b was used. The model dimensions drawn into the simulation software are shown in Fig. 3. All boundaries labeled in Fig. 3 were defined with a “no-slip” condition, with the exception of the edges labeled “A” and “B”. Edge “A” was defined with an inflow  $y$ -velocity of  $1.042\text{ m/s}$  and “B” was set with an outflow pressure at atmospheric pressure.

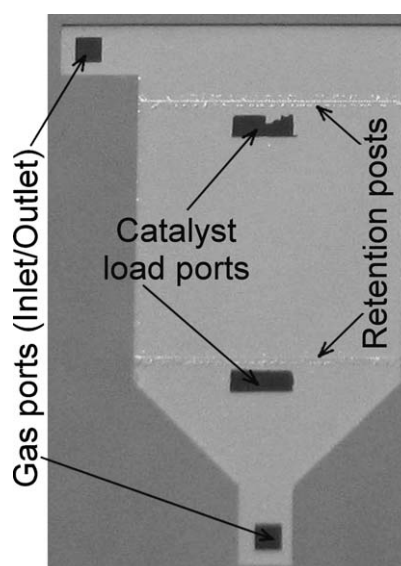
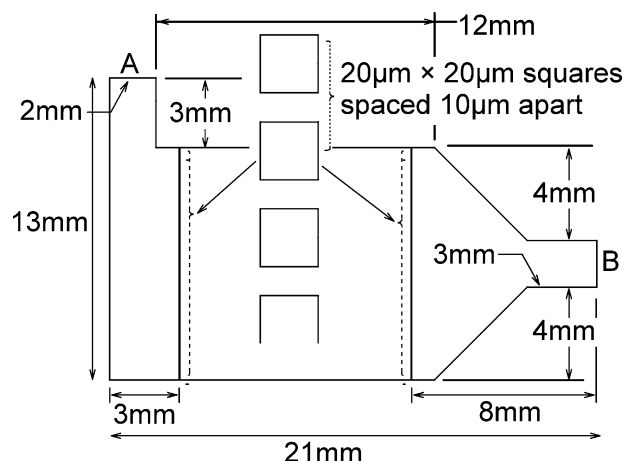


Fig. 2. Photograph of the Si microreactor used in this study.



**Fig. 3.** Dimensions of the simulated microreactor. Inlet and outlet sections are labeled as “A” and “B”; positions of retention posts are shown along with a close up of the retention post geometry.

Details of the retention posts and the positions relative to the edges are also given in Fig. 3. In order to simplify the computations, the fluid was modeled with an incompressible Navier–Stokes model, using flowing air (50 sccm) at atmospheric pressure and room temperature.

### 2.3. In situ IR study

#### 2.3.1. Studies using a conventional MCT detector

Spectra were collected in a Nicolet Magna-860 equipped with a mercury cadmium telluride (MCT) detector (MCT-B, Thermo Electron). Collection parameters were set at a resolution of  $4\text{ cm}^{-1}$  (corresponding to data spacing of  $\sim 2\text{ cm}^{-1}$ ) averaging over 16 scans with the mirror velocity at  $1.8988\text{ cm/s}$ . Samples to be analyzed were placed in the sample compartment of the instrument for transmission studies.

#### 2.3.2. Studies using a focal plane array (FPA) MCT detector

Spatially resolved FTIR spectra were obtained using an experimental and optical system very similar to one previously described in the literature [10]. A  $128 \times 128$  pixel MCT focal plane array (SBF-161, Santa Barbara Focal Plane, Goleta CA) was used in conjunction with the Nicolet Magna-860 FTIR spectrometer. The optical setup provided an analysis dimension of about  $400\text{ }\mu\text{m} \times 400\text{ }\mu\text{m}$  for each pixel. The FPA was driven at a frame capture rate of 1600 Hz while running the FTIR at a mirror velocity of  $0.3165\text{ cm/s}$  and a resolution of  $4\text{ cm}^{-1}$ . The trigger from the FTIR was first passed to a custom built trigger box which delays the periodic TTL (transistor-transistor logic) signal by a factor of 8 (i.e. 1 trigger gets passed on for every 8). This forced delay allows the FPA time to transfer the data for each captured spectrum to the computer. With these parameters, 2484 frames were required to describe a full spectrum over a range up to  $2527\text{ cm}^{-1}$  [38]. Raw data from the FPA was captured using WinIR 3.7.0.0 (Santa Barbara Focal Plane, Goleta CA). Data were processed post capture using a combination of custom JAIMP (Just Another Image Manipulation Program) software for transforming and averaging [39], as well as in-house written software to extract and process data. Each FPA spectrum here was averaged over 6 scans and corrected using a triangular apodization. The y-positions given in this paper are relative and the larger the number, the further along the vertical position the point is away from the gas inlet. Similarly, the x-positions are relative and the larger numbers indicate a position further away from the gas inlet along the horizontal axis. For reference, the center pixel at the location of the gas inlet was

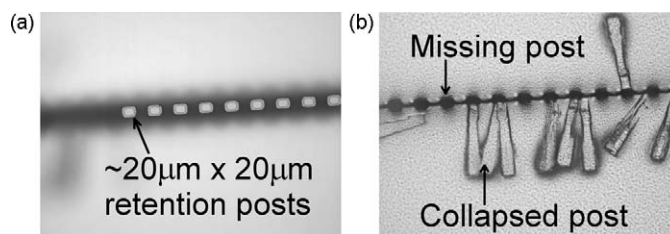


**Fig. 4.** Optical micrographs after the fabrication process which illustrate (a) surviving retention posts and (b) collapsed posts.

determined to be at (32, 34). The actual capture of each spectrum series required about 1 min.

### 2.4. Catalyst integration and packaging

2.98 wt% Pt dispersed on a  $\text{SiO}_2$  support prepared by Dr. Jeffrey T. Miller (Argonne National Labs) was investigated. The catalysts were made by dispersing 10 g of Davisil 646 Silica (Aldrich, surface area of  $300\text{ m}^2/\text{g}$  with  $1.1\text{ cm}^3/\text{g}$  pore volume) in 50 mL of  $\text{H}_2\text{O}$  and 2 mL of  $\text{NH}_4\text{OH}$  to form a slurry. A separate solution containing Pt ( $0.60\text{ g Pt}(\text{NH}_3)_4(\text{NO}_3)_2$  dissolved in 25 mL of  $\text{H}_2\text{O}$  and 2 mL of  $\text{NH}_4\text{OH}$ ) was added quickly into the continuously agitated slurry. After 15 min, the catalyst was filtered and washed with  $\text{H}_2\text{O}$  and dried at  $125\text{ }^\circ\text{C}$ . The dried catalyst was reduced with  $\text{H}_2$  by rapidly heating from room temperature to  $150\text{ }^\circ\text{C}$  in  $\text{H}_2$  and holding for

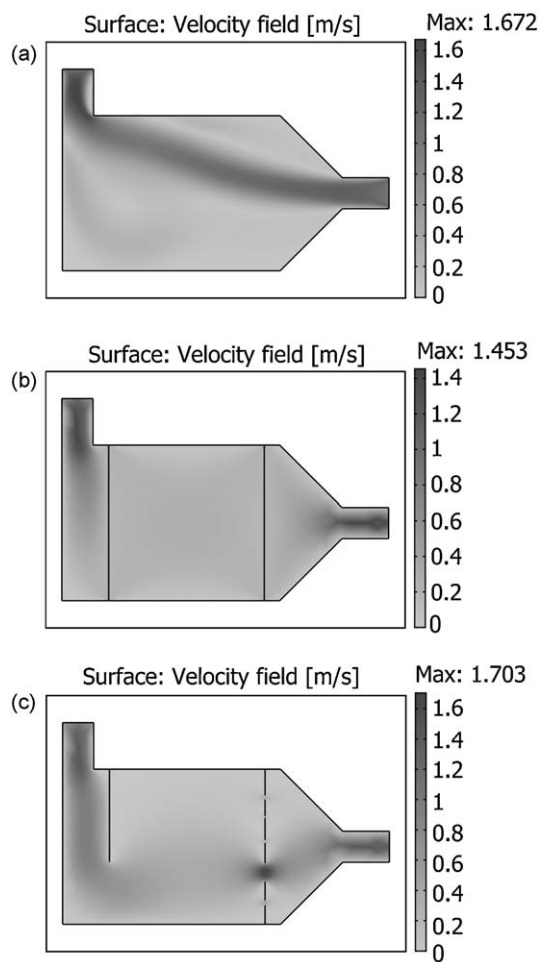


**Fig. 5.** Finite element simulations of gaseous flow in the microreactor at steady state with (a) no retention posts, (b) all retention posts intact and (c) selected retention posts missing.

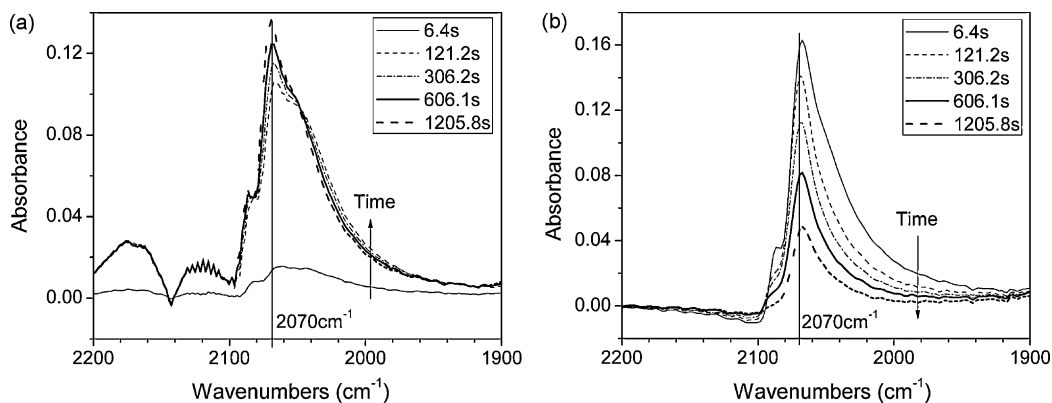


**Fig. 6.** FTIR spectra as a function of time characterizing CO adsorbed on a Pt/SiO<sub>2</sub> catalyst washcoated in a silicon microreactor during (a) CO adsorption (100% CO, room temperature) and (b) CO oxidation (2.5% O<sub>2</sub>/N<sub>2</sub>, room temperature).

30 min. Completion of the reduction occurred by increasing the temperature to 250 °C and holding for 30 min, then switching to He gas and cooling to room temperature. Analysis of the final catalyst was determined to be 2.98% with a dispersion of 53%.

The catalyst powder was initially drawn into the microreactor channel using vacuum suction [40]. The channel was then filled with deionized water using a micropipette at room temperature and dried on a hotplate at ~80 °C. A second Pt/SiO<sub>2</sub> washcoat was added by dispersing the powdered catalyst in water (1:2 by volume, catalyst:water) and injecting the slurry into the channel using a micropipette until overflow occurred. The microreactor was heated on the hotplate at 80 °C to dry, and the slurry fill process was repeated an additional 2 times. Total catalyst loading was weighed to be ~7.05 mg using a Mettler Toledo XS205 microbalance. For packaging, 1/16" stainless steel tubing was attached to the inlet and outlet gas ports using epoxy (Loctite<sup>®</sup>, Quick Set<sup>™</sup>) to the points of contact. Catalyst ports were sealed with epoxy-covered tape. Gaseous flows through the packaged system were measured and verified under bypass conditions to ensure a hermetic seal at room temperature.

### 2.5. CO oxidation

The catalyst was pre-treated at room temperature using 50 cm<sup>3</sup>/min gas flow after being loaded and sealed in the microreactor. Pre-treatment included exposure to 100% O<sub>2</sub> (Praxair, 4.3 UHP) for 10 min, followed by a N<sub>2</sub> purge for 2 min, and 100% H<sub>2</sub> (Praxair, 5.0 UHP) for >30 min. This treatment served to clean the catalyst surface of any adsorbed CO, as confirmed by

the absence of CO adsorption peaks in the single beam background spectra (not shown). CO adsorption was carried out using either 100% CO (Matheson, UHP) or 1000 ppm CO/He (Praxair). After CO adsorption, the reactor was purged with N<sub>2</sub> for 20 min to desorb physisorbed CO. Subsequent CO oxidation was carried out using 2.5% O<sub>2</sub>/N<sub>2</sub> (O<sub>2</sub> as above, N<sub>2</sub> from liquid nitrogen off gas). Quantifications of the areas under the spectral bands were obtained through direct integration of the area under the obtained peaks. The microreactor-loaded catalyst was maintained in inert gas flow between experiments and then subjected to the same pre-treatment procedures described above to obtain reproducibility between runs.

## 3. Results

### 3.1. Microreactor characterization

The microreactor design contains 20 μm long by 20 μm wide retention posts spaced 10 μm apart to retain catalyst within the reaction chamber and to distribute gas flow uniformly across the reactor width. Fig. 4 shows optical micrographs of retention posts after DRIE and LTO removal. Many posts survived the processing (Fig. 4(a)); however, some collapsed (Fig. 4(b)) upon loss of mechanical stability likely resulting from degradation of the post width (<20 μm) when scalloping occurs during DRIE [41]. With only part of the retention posts intact, the flow of gases through the microreactor is not expected to be completely uniform.

The effect of retention post density on gas flow and channeling was simulated and Fig. 5 shows the finite element results. Fig. 5(a)

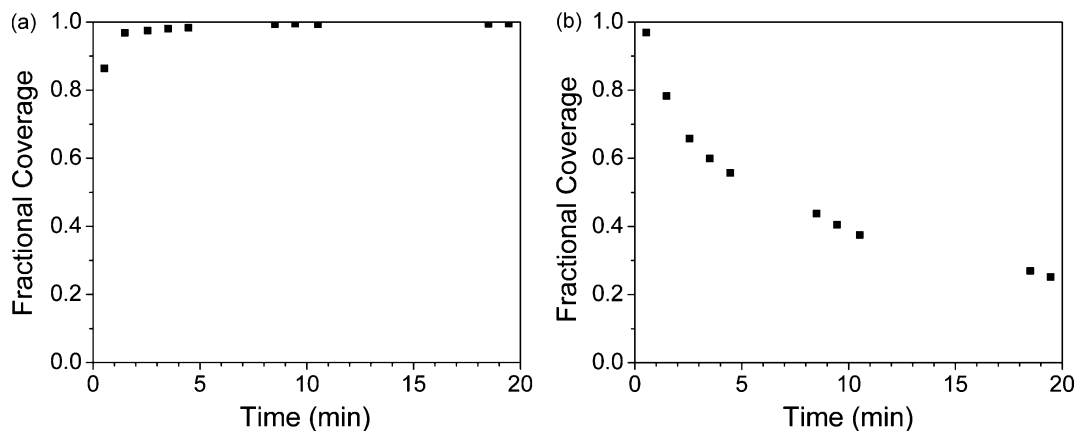


**Fig. 7.** Fractional CO coverage as a function of time on a Pt/SiO<sub>2</sub> catalyst washcoated in a silicon microreactor during (a) pure CO adsorption at room temperature, 50 cm<sup>3</sup>/min and (b) CO oxidation (2.5% O<sub>2</sub>/N<sub>2</sub>, room temperature, 51 cm<sup>3</sup>/min).

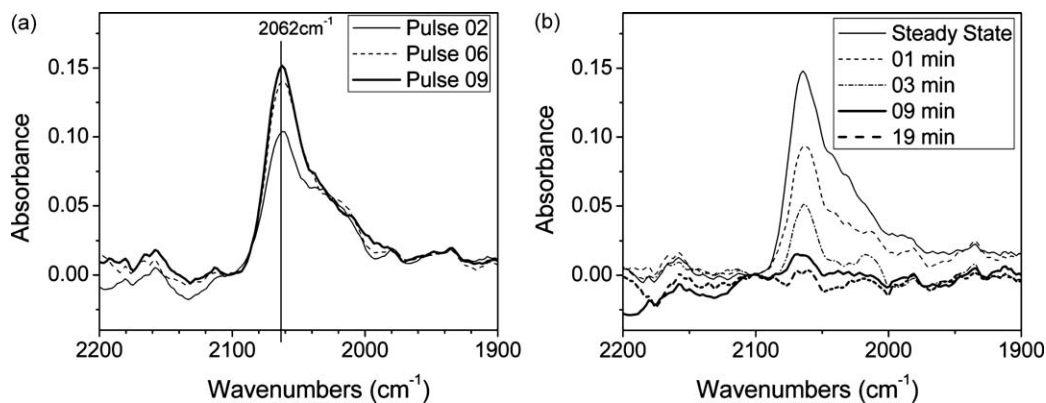


Fig. 8. FPA-FTIR spectra of CO adsorbed on Pt/SiO<sub>2</sub> at position (45, 52) as a function of pulse number during (a) CO adsorption and (b) CO oxidation, both at room temperature.

shows the situation with no retention posts; clear channeling of inlet gases directly to the outlet port is observed. The addition of uniform retention posts (10 μm spacing) near the inlet and outlet distributes the flow of gases evenly over the entire reactor width (Fig. 5(b)) as intended. In the case where only some of the retention posts are present, the gas flow distribution contains non-ideality, as shown in Fig. 5(c). The distribution of the gaps in the retention posts in the fabricated microreactor is expected to be random and could not be characterized after packaging. Although the precise flow distribution depends on the exact post distribution, it is expected that the flow of gases through this particular microreactor was not uniform, i.e. some channeling through the reactor likely occurred. However, regardless of the post distribution, gas was still distributed across the reactor width, just at different flow rates. Dead volumes were not apparent in any case. Implications of the non-uniform flow pattern on FTIR analysis is discussed in a later section.

### 3.2. FTIR of CO adsorption on Pt/SiO<sub>2</sub> – microreactor with a conventional MCT detector

CO adsorption (using 100% CO) at room temperature over a Pt/SiO<sub>2</sub> washcoat in the microreactor as a function of time is shown in Fig. 6(a). Subsequent oxidation of adsorbed CO using 2.5% O<sub>2</sub>/N<sub>2</sub> is shown in Fig. 6(b). These spectra were collected using a MCT-B detector with the IR beam irradiating the entire area of the microreactor, which was placed in the sample compartment of the FTIR spectrometer. Thus, each spectrum characterizes the average CO adsorbed over the entire plane of Pt/SiO<sub>2</sub> contained in the microreactor (no spatial resolution). Linear CO adsorbed on Pt is observed at ~2070 cm<sup>-1</sup>, consistent with observations in the literature [42–48]. The shoulder present at ~2085 cm<sup>-1</sup> is also consistent with reported observations [45]. The identity of the shoulder at ~2085 cm<sup>-1</sup> has not been agreed upon in the literature [48], having been attributed to linear CO adsorbed on Pt in small mats or arrays [49,50] or on a Pt<sup>δ+</sup> site [44,51]. The corresponding CO fractional coverages during CO adsorption and oxidation, calculated as a ratio of the area under the linear CO band relative to that at CO saturation, are shown in Fig. 7. The CO oxidation rate at room temperature is reflected by the slope of the decay curve in Fig. 7(b).

### 3.3. FTIR of CO adsorption on Pt/SiO<sub>2</sub> – microreactor with a FPA-MCT detector

To spatially resolve and capture propagation of a CO adsorption front travelling down the length of the microreactor, CO was adsorbed using pulses of 1000 ppm CO/He at ~15 cm<sup>3</sup>/min for 15 s (corresponding to ~0.14 theoretical monolayers of CO per pulse) intermittently between N<sub>2</sub> gas flow segments. This method was

performed to accommodate the 1 min capture rate currently limiting the FPA system. After 10 pulses, 1000 ppm CO was flowed over the catalyst to allow adsorption for 10 min to fully saturate the surface adsorption sites.

Spectra monitoring CO adsorption and oxidation at room temperature at FPA pixel position  $x = 45, y = 52$  are shown in Fig. 8. Each pixel obtained in the FPA-FTIR setup corresponds to an area approximately 400 μm by 400 μm on the microreactor system being analyzed. The strongest linear CO bands in the FPA spectra fall around 2070 cm<sup>-1</sup>, consistent with the conventional FTIR results (Section 3.2) as well as values reported in literature. At any single FPA pixel and microreactor position, one can monitor, using the linear CO band, both CO uptake and CO oxidation with good signal to noise ratio.

In order to spatially resolve and monitor CO adsorption and oxidation propagation down the microchannel length, one must

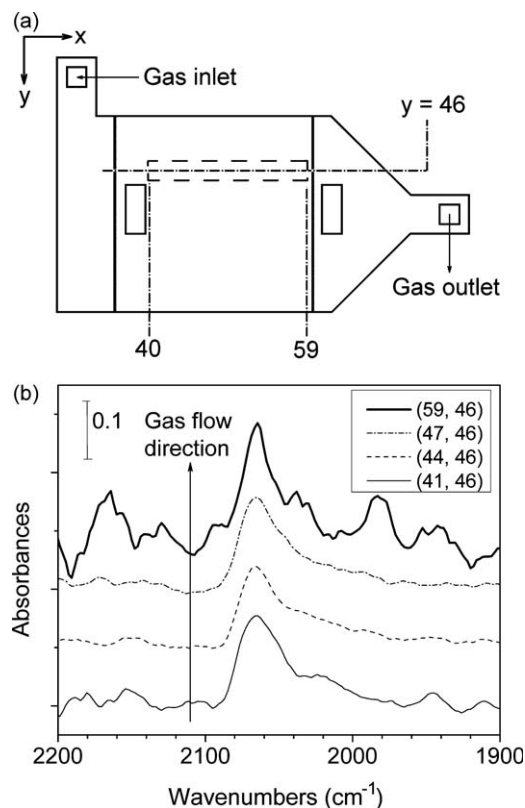


Fig. 9. FTIR analysis of a CO-saturated Pt/SiO<sub>2</sub> surface at room temperature at various microreactor positions, (a) schematic describing FPA pixel locations and (b) corresponding FTIR spectra.

compare a series of spectra at identical time or pulse numbers but at different positions. One regime investigated for this purpose along  $y = 46$  is shown in Fig. 9(a). Fig. 9(b) shows FTIR spectra of CO adsorbed on Pt/SiO<sub>2</sub> after saturation as a function of reactor channel location ( $x = 41$ –59) in this region within the microreactor. Each spectrum represents data obtained from a single pixel. Absolute absorbances at saturation are not the same at each position due to a combination of factors including variations in the catalyst thickness and MCT detector response with pixel position.

FTIR spectra of CO adsorption during pulse chemisorption are shown in Fig. 10 for the previously mentioned axial position in the microreactor, corresponding to segments shown in Fig. 9. Pulsing experiments were conducted in order to demonstrate the ability of the system to spatially resolve the progression of CO adsorption to near saturation down the length of the microreactor. Upon introduction of CO pulses to the reactor, adsorption was initially observed at pixels (41, 46) as this is the position nearest to the gas inlet port. The amount of linearly bound CO at this position increases with increasing pulse number and nearly reach its saturation value by pulse number 8 upon introduction of  $1.33 \times 10^{-6}$  moles of CO (refer to the saturation spectra in Fig. 9(b)). As more CO pulses are introduced, absorption peaks for linearly bound CO are observed with increasing intensity at pixel positions (44, 46) and (47, 46), which extend further down the reactor channel. Even after 9 consecutive pulses, CO has not yet reached pixel (59, 46) near the end of the reactor. In this washcoated system, the CO flow through the reaction channel will be highly axially dispersed, allowing CO to adsorb on the catalyst surface at positions further down the channel before the inlet segments of the catalyst surface are saturated. As the

catalyst closer to the inlet saturates, more CO will be available at longer channel lengths and the rate of uptake further down will increase. This phenomena is captured by the microreactor/FPA system.

Since the catalyst thickness in the microreactor is most likely not completely uniform throughout, and thus, the attenuation of the transmitted IR beam will not be the same at each position, fractional coverages (relative to complete saturation at a given pixel position) were used as a basis for normalization after each pulse. Similar to the analysis performed on the conventional FTIR data (see Fig. 7) this normalization is done by obtaining the integrated area under the linear CO band for the steady state signal, then normalizing all the other peak areas to the steady state area. Fig. 11(a) shows the fractional CO coverage during adsorption at  $y$ -positions 46 (corresponding to data in Fig. 10). Positions closer to the inlet gas port saturate sooner (in fewer CO pulses) than points further down the channel and along the same horizontal position.

After CO adsorption to saturation throughout the reactor and N<sub>2</sub> purging at room temperature, 2.5% O<sub>2</sub> in N<sub>2</sub> was introduced at room temperature to oxidize the adsorbed CO to CO<sub>2</sub>. Fig. 12 shows the absorbance due to linearly bound CO during oxidation of CO previously adsorbed on the Pt surface. FPA data in Fig. 12 are shown for position  $y = 46$  as a function of oxidation time.  $x$ -positions 41, 44, and 47 are separated by about 1 mm each, and  $x$ -position 59 is near the channel end. Again, the amount of linearly bound CO is characterized by the intensity or area of the peak centered at  $\sim 2070$  cm<sup>-1</sup>. Due to sensitivity limitations of the FPA system, the small shoulder present  $\sim 2080$  cm<sup>-1</sup> (and seen in Fig. 6) cannot be resolved. At shorter times, the amount of CO adsorbed decreases at the pixel position closer to the inlet, followed by propagation of oxidation to locations further down the reactor at a

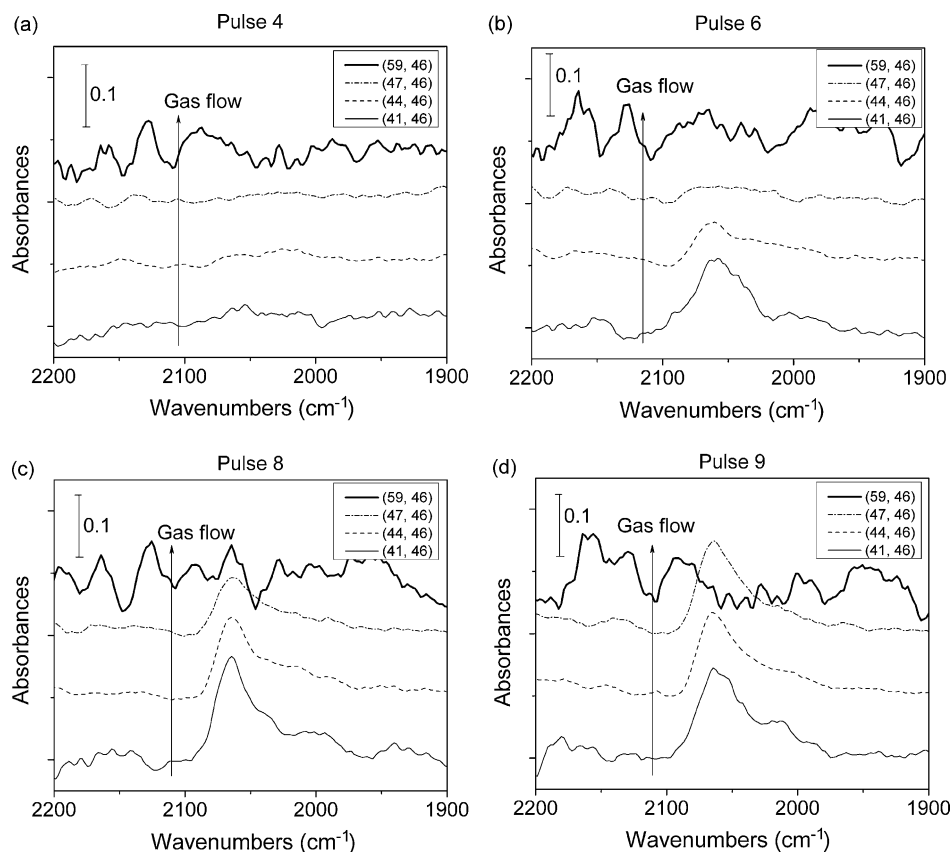


**Fig. 10.** FPA-FTIR spectra of CO adsorbed on Pt/SiO<sub>2</sub> at room temperature as a function of microreactor position and pulse number for  $y = 46$ . Note that position (41, 46) is near the reactor inlet and position (59, 46) is near the reactor outlet as shown in this figure.

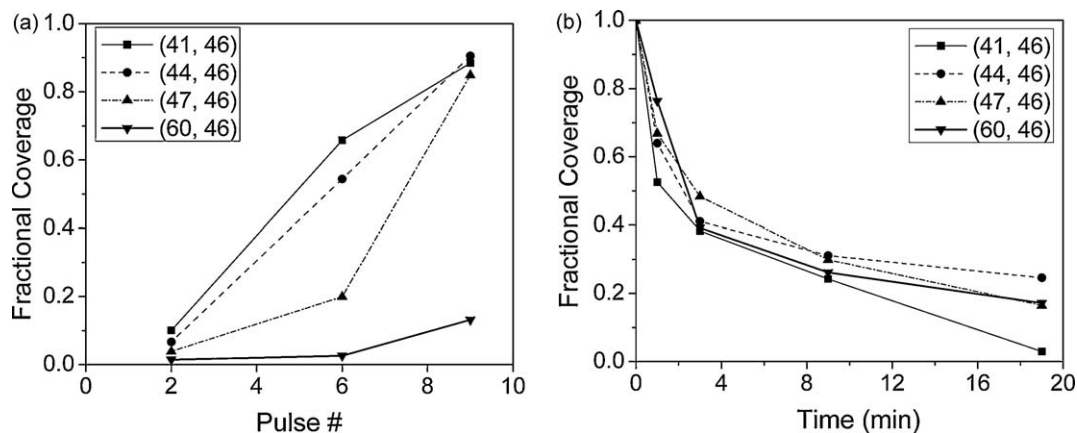


Fig. 11. Normalized room temperature CO coverage at different  $x$ -positions along  $y = 46$  during (a) CO adsorption and (b) oxidation.

later time. These results clearly show changes in CO coverage as a function of position and time during a catalytic reaction. Fig. 11(b) shows fractional CO coverage during oxidation (at position  $y = 46$ ) and clarifies that CO coverage decreases faster at earlier channel locations.

### 3.4. Flow characteristics from FPA data quantification

Fig. 13 shows CO fractional coverage as a function of pulse number during CO adsorption at a designated  $x$ -position and variable  $y$ -position. Thus, each of Fig. 13(a–c) represents a different vertical segment of the microreactor perpendicular to the flow direction. These results confirm that the gas flow through the microreactor is not uniform across the microreactor width, as

predicted by the absence of some catalyst retention posts. With a completely uniform flow through the microreactor, the fractional coverage along the same  $x$ -position would be expected to rise at almost exactly the same rate at each  $y$ -position. We note that such non-uniform flow behavior of gases would not be observed by conventional FTIR techniques because spectra are averaged over the entire sample.

Even with lost catalyst retention and gas distribution posts, the gas flow from the inlet will not completely channel through one area. Rather, the flows at each  $y$ -position will be slightly different and each pixel position should still capture propagating CO adsorption and oxidation events. As the presented results show for purposes of demonstrating these capabilities, spatially resolved adsorption and oxidation of CO is clearly observed despite the

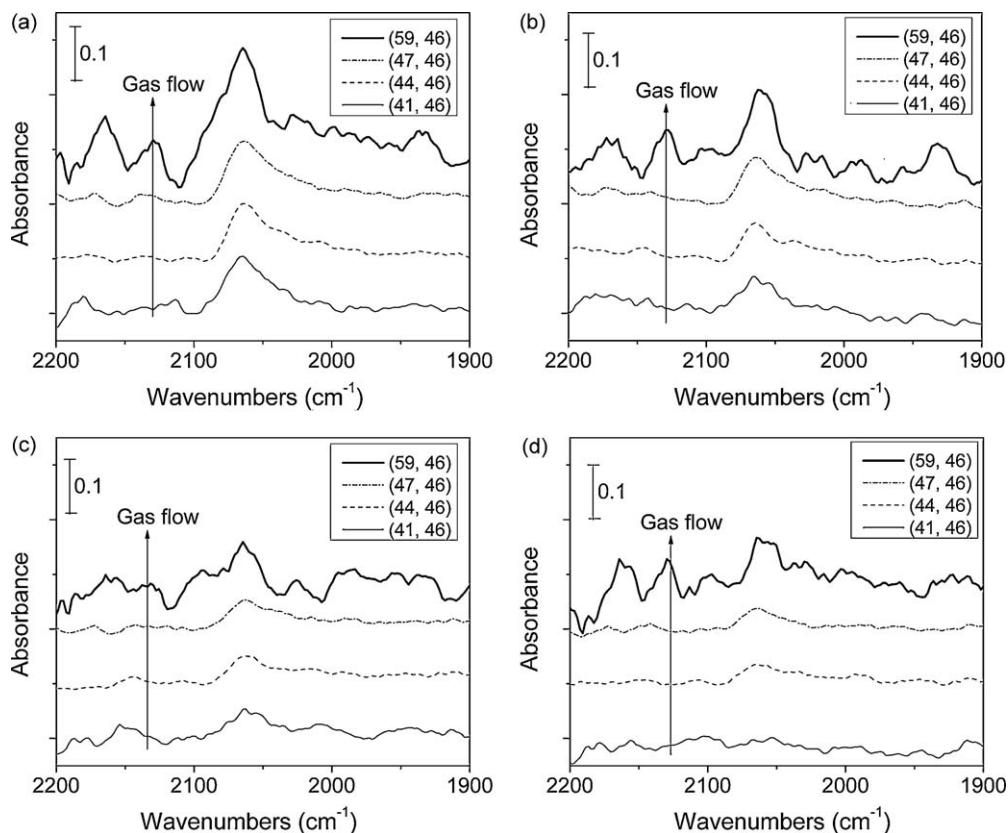


Fig. 12. Spectral response as a function of time during the room temperature oxidation of adsorbed CO using 2.5% O<sub>2</sub>/N<sub>2</sub>; data at times (a) 1 min, (b) 3 min, (c) 9 min and (d) 19 min.

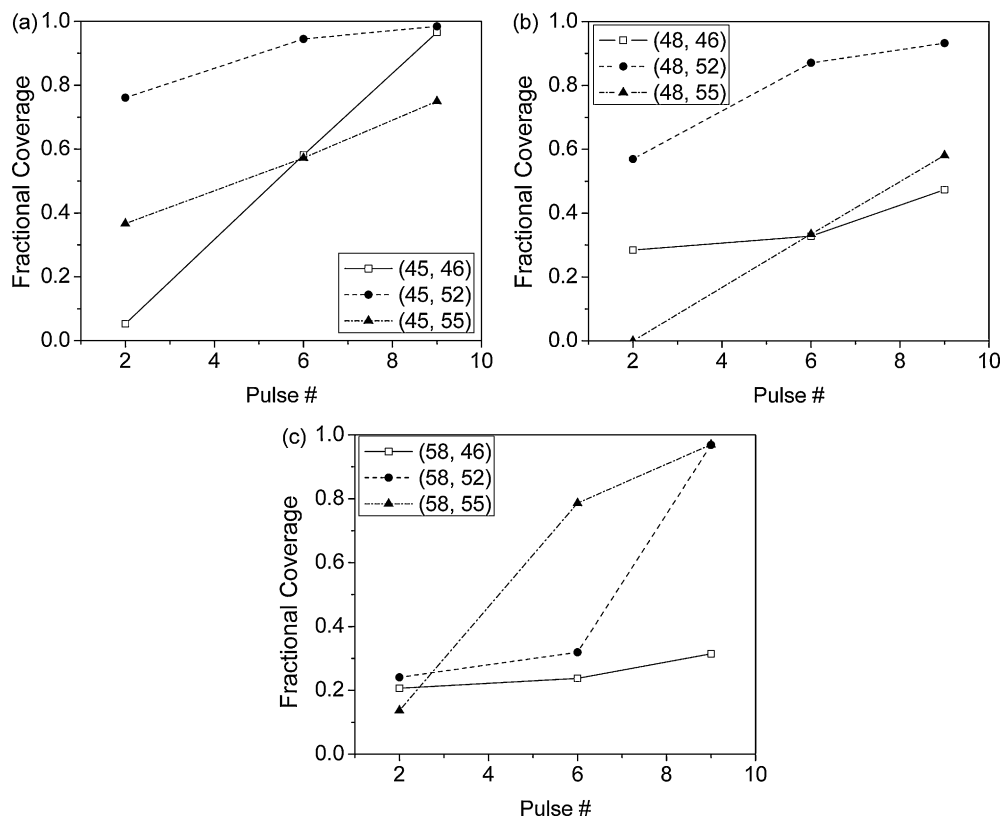


Fig. 13. Normalized data (CO coverages) at different positions during room temperature CO pulsing at (a)  $x=45$ , (b)  $x=48$  and (c)  $x=58$ .

presence of small flow non-uniformities. The microreactor design and fabrication can readily be improved upon to remove this non-uniformity and artifact, particularly by using a reactor with a series of parallel channels mimicking a monolith stack.

### 3.5. Comparison of FPA-MCT and conventional MCT results

As the array size for analysis is increased in the FPA (beyond a single pixel), spectral analysis in the microreactor should approach that obtained using the conventional MCT system. Fig. 14 shows the fractional coverage of CO during oxidation at room temperature obtained from the two detector systems. The data from the FPA-MCT detector system were obtained from a rectangular 72

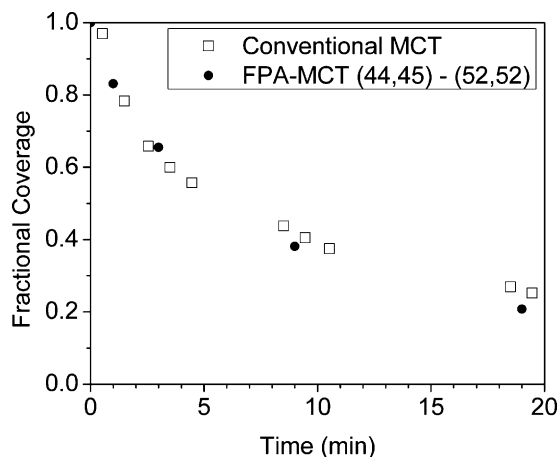


Fig. 14. Normalized CO coverage during oxidation at room temperature with IR detection measured using a conventional MCT detector ( $\square$ ) and a FPA-MCT detector ( $\bullet$ ).

pixel domain averaged from (44, 45) to (52, 52). Comparison of results previously shown in Figs. 6 and 8 shows that the signal to noise ratio of the conventional MCT detector used is superior to that of the FPA-MCT detector system. Peaks are sharper and shoulders are better defined at identical catalyst conditions. However, from Fig. 14 it is clear that key catalyst kinetics are equally captured by both detectors.

## 4. Conclusions

These results illustrate the capability of silicon microreactors coupled with an FPA-FTIR system for the spatially resolved transient analysis of surface species over a catalyst. The example of CO adsorption and oxidation over a Pt catalyst was used. Both the propagation of adsorbed CO down the microchannel during pulse chemisorption and subsequent propagating oxidation of CO to  $\text{CO}_2$  were observed and characterized. By applying microreactors operated in such a manner for catalytic studies of monolithic systems, one can quantify both surface species and gas phase product information (via connection to an external instrument at the effluent in the simplest case) simultaneously. Further, the microreactor-imaging system demonstrated here enables simultaneous imaging of the entire catalytic bed under reaction conditions. A comparison of CO oxidation on Pt in a silicon microreactor using a conventional FTIR versus an FPA-FTIR imaging system showed that the FPA provides identical kinetic results with the added capability of spatial resolution. The spectra given in this paper show that each data point obtained by the FPA is unique and wholly dependent on the nature of the reactor and catalyst at each point. One promising future application of this approach is to the study of  $\text{NO}_x$  reactions in a monolithic reactor to better elucidate the mechanistic steps during reaction. Replicating the channels of monolithic reactors used in automobiles is well within the bounds of standard microfabrication technologies.

## Acknowledgements

Funding was provided by the National Science Foundation (CBET # 0828852) and the Indiana 21st Century Fund in collaboration with Cummins Inc. The authors acknowledge staff of the Birck Nanotechnology Center for their fabrication support and Dr. Jeffrey T. Miller for the preparation and supply of catalysts.

## References

- [1] N. Takahashi, H. Shinjoh, T. Iijima, T. Suzuki, K. Yamazaki, K. Yokota, H. Suzuki, N. Miyoshi, S. Matsumoto, T. Tanizawa, *Catal. Today* 27 (1996) 63–69.
- [2] J.A. Anderson, A.J. Paterson, M. Fernandez-Garcia, *Stud. Surf. Sci. Catal.* 130B (2000) 1331–1336.
- [3] H. Abdulhamid, J. Dawody, E. Fridell, M. Skoglundh, *J. Catal.* 244 (2006) 169–182.
- [4] S. Balcon, C. Potvin, L. Salin, J.F. Tempere, G. Djega Mariadassou, *Catal. Lett.* 60 (1999) 39–43.
- [5] W.S. Epling, L.E. Campbell, A. Yezerets, N.W. Currier, J.E. Parks II, *Catal. Rev.-Sci. Eng.* 46 (2004) 163–245.
- [6] K.S. Kabin, R.L. Muncrief, M.P. Harold, *Catal. Today* 96 (2004) 79–89.
- [7] J.S. Choi, W.P. Partridge, C.S. Daw, *Appl. Catal. A* 293 (2005) 24–40.
- [8] J.S. Choi, W.P. Partridge, W.S. Epling, N.W. Currier, T.M. Yonushonis, *Catal. Today* 114 (2006) 102–111.
- [9] C.M. Snively, J. Lauterbach, *Spectroscopy* 17 (2002) 26–33.
- [10] C.M. Snively, G. Oskarsdottir, J. Lauterbach, *Catal. Today* 67 (2001) 357–368.
- [11] C.M. Snively, G. Oskarsdottir, J. Lauterbach, *Angew. Chem., Int. Ed.* 40 (2001) 3028–3030.
- [12] C.M. Snively, C. Pellerin, J.F. Rabolt, D.B. Chase, *Anal. Chem.* 76 (2004) 1811–1816.
- [13] R.J. Hendershot, R. Vijay, C.M. Snively, J. Lauterbach, *Chem. Eng. Sci.* 61 (2006) 3907–3916.
- [14] J.A. Lauterbach, C.M. Snively, J.P. Dicke, G. Oskarsdottir, *International Patent WO 01/06209 A1*, 2001.
- [15] C. Pellerin, C.M. Snively, D.B. Chase, J.F. Rabolt, *Appl. Spectrosc.* 58 (2004) 639–646.
- [16] A. Bourane, D. Bianchi, *J. Catal.* 220 (2003) 3–12.
- [17] A. Bourane, S. Derrouiche, D. Bianchi, *J. Catal.* 228 (2004) 288–297.
- [18] A. Bourane, D. Bianchi, *J. Catal.* 222 (2004) 499–510.
- [19] R. Herzig-Marx, K.T. Queeney, R.J. Jackman, M.A. Schmidt, K.F. Jensen, *Anal. Chem.* 76 (2004) 6476–6483.
- [20] S. Loebbecke, W. Schweikert, T. Tuercke, J. Antes, E. Marioth, H. Krause, in: *Proceedings of the International Conference on Microtechnologies: MICRO.tec 2000*, Hannover, Germany, (2000), pp. 789–791.
- [21] P.D.I. Fletcher, S.J. Haswell, X. Zhang, *Electrophoresis* 24 (2003) 3239–3245.
- [22] H. Lu, M.A. Schmidt, K.F. Jensen, in: *Proceedings of the 2nd Annual International IEEE-EMBS Special Topic Conference on Microtechnologies in Medicine and Biology*, Piscataway, NJ, USA, (2002), pp. 462–465.
- [23] L. Olsson, B. Westerberg, H. Persson, E. Fridell, M. Skoglundh, B. Andersson, *J. Phys. Chem. B* 103 (1999) 10433–10439.
- [24] L. Olsson, H. Persson, E. Fridell, M. Skoglundh, B. Andersson, *J. Phys. Chem. B* 105 (2001) 6895–6906.
- [25] M. Crocoll, S. Kureti, W. Weisweiler, *J. Catal.* 229 (2005) 480–489.
- [26] H. Mahzoul, J.F. Brilliac, P. Gilot, *Appl. Catal. B* 20 (1999) 47–55.
- [27] E. Fridell, H. Persson, B. Westerberg, L. Olsson, M. Skoglundh, *Catal. Lett.* 66 (2000) 71–74.
- [28] I. Nova, L. Lietti, L. Castoldi, E. Tronconi, P. Forzatti, *J. Catal.* 239 (2006) 244–254.
- [29] B.R. Kromer, L. Cao, L. Cumarantunge, S.S. Mulla, J.L. Ratts, A. Yezerets, N.W. Currier, F.H. Ribeiro, W.N. Delgass, J.M. Caruthers, *Catal. Today* 136 (2008) 93–103.
- [30] N. Maluf, K. Williams, *An Introduction to Microelectromechanical Systems Engineering*, second ed., Artech House, Inc., Norwood, MA, 2004.
- [31] S.A. Campbell, *The Science and Engineering of Microelectronic Fabrication*, second ed., Oxford University Press, 2001.
- [32] W.B. Yu, C.M. Tan, J. Wei, S.S. Deng, M.L. Nai, in: *Proceedings of the 5th Electronics Packaging Technology Conference (EPTC 2003)*, Singapore, (2003), pp. 294–297.
- [33] Q.Y. Tong, U. Gosele, first ed., *Semiconductor wafer bonding: science and technology*, John Wiley & Sons, New York, 1999, pp. 103–117.
- [34] E. Cao, W.B. Motherwell, A. Gavriilidis, *Chem. Eng. Technol.* 29 (2006) 1372–1375.
- [35] R. Srinivasan, I.-M. Hsing, P.E. Berger, K.F. Jensen, S.L. Firebaugh, M.A. Schmidt, M.P. Harold, J.J. Lerou, J.F. Ryley, *AIChE J.* 43 (1997) 3059–3069.
- [36] K. Kusakabe, D. Miyagawa, Y. Gu, H. Maeda, S. Morooka, *J. Chem. Eng. Jpn.* 34 (2001) 441–443.
- [37] P.T. Fanson, M.R. Horton, W.N. Delgass, J. Lauterbach, *Appl. Catal. B* 46 (2003) 393–413.
- [38] C.M. Snively, J. Lauterbach, *Appl. Spectrosc.* 59 (2005) 1075–1081.
- [39] S.S. Lasko, Master's Thesis, Purdue University, West Lafayette, 2002.
- [40] S.K. Ajmera, C. Delattre, M.A. Schmidt, K.F. Jensen, *J. Catal.* 209 (2002) 401–412.
- [41] A.A. Ayon, K.S. Chen, K.A. Lohner, S.M. Spearing, H.H. Sawin, M.A. Schmidt, *Mater. Res. Soc. Symp. Proc.* 546 (1999) 51–61.
- [42] J.D. Heno, T. Caputo, J.H. Yang, M.C. Kung, H.H. Kung, *J. Phys. Chem. B* 110 (2006) 8689–8700.
- [43] P.T. Fanson, PhD Dissertation, Purdue University, West Lafayette, 2002.
- [44] P.T. Fanson, W.N. Delgass, J. Lauterbach, *J. Catal.* 204 (2001) 35–52.
- [45] A. Bourane, D. Bianchi, *J. Catal.* 209 (2002) 126–134.
- [46] D.J. Kaul, E.E. Wolf, *Chem. Eng. Sci.* 41 (1986) 1101–1107.
- [47] S.G. Podkolzin, J. Shen, J.J. De Pablo, J.A. Dumesic, *J. Phys. Chem. B* 104 (2000) 4169–4180.
- [48] A. Bourane, D. Bianchi, *J. Catal.* 218 (2003) 447–452.
- [49] J.A. Anderson, C.H. Rochester, *J. Chem. Soc., Faraday Trans.* 87 (1991) 1479–1483.
- [50] O. Dularent, D. Bianchi, *Appl. Catal. A* 196 (2000) 271–280.
- [51] R.K. Herz, E.J. Shinouskis, *Appl. Surf. Sci.* 19 (1984) 373–397.